Turkish Journal of Electrical Engineering & Computer Sciences

http://journals.tubitak.gov.tr/elektrik/

Research Article

Turk J Elec Eng & Comp Sci
(2016) 24: 3638 – 3651

doi:10.3906/elk-1406-120

A current feedback control strategy for parallel-connected single-phase inverters using a third-order general-integrator crossover cancellation method

Yuan HUANG[1,2,*], **An LUO**[1]

[1]National Electric Power Conversion and Control Engineering Technology Research Center, Hunan University, Changsha, China

[2]College of Information and Electrical Engineering, Hunan University of Science and Technology, Changsha, China

Received: 18.06.2014 • **Accepted/Published Online:** 26.05.2015 • **Final Version:** 20.06.2016

Abstract: Virtual impedance is usually introduced to the control system of parallel inverters in order to change the inverter equivalent output impedance and to enhance control accuracy and power sharing. In this paper, a current feedback control strategy using a third-order general-integrator crossover-cancellation method that can be implemented in a virtual impedance loop is proposed. This method consists of 2 parts: a crossover-cancellation feedback network, which achieves the band-pass effect, and a multilevel TOGI-OSG link, which acts as a filter. Compared with the conventional virtual impedance method, the proposed method can avoid derivation of output current, reduce system calculating burden, and enhance dynamic response. Additionally, this method can reduce the THD of output voltage in the case of nonlinear load and can also drastically restrain the impact of DC component on output voltage. A prototype consisting of 2 sets of 2-kW photovoltaic inverters operating in parallel was built in the laboratory. Simulated and experimental results are examined to verify the effectiveness and feasibility of this method.

Key words: Microgrid, island mode, parallel inverter, droop control, virtual impedance

1. Introduction

With the coordinated development of global exploitation of energy with environmental protection, acceleration of research on microgrid technology is of great practical significance for efficient utilization of new energy [1–3]. A microgrid is a system consisting of distributed generation and load that can operate in both grid-connected mode and islanded mode. Therefore, research on control technology for parallel inverters in the islanded mode of a microgrid is very important, as it would greatly improve output power quality and overall capacity, and also enhance redundancy and reliability.

In recent years, many scholars have focused on control methods for parallel inverters. Droop control methods [4–7] have been widely applied due to the advantages of not requiring the use of a communication line, high reliability, flexible operation, etc. However, the traditional droop control method has inherent defects including slow dynamic response and low steady-state current-sharing accuracy; furthermore, the power sharing accuracy is highly sensitive to the inverter output impedance, which is determined by the adopted control method and system parameters [8,9]. Therefore, improved droop control methods have been proposed in many works. In [10–15], "virtual impedances" are introduced to the current feedback loop of the control system. By configuring virtual impedances presenting resistive [11], inductive [12], and complex impedance [13,14] characteristics, the

*Correspondence: hy_8615381@163.com

inverter equivalent output impedance can be conveniently regulated to enhance the control accuracy and to improve power sharing among parallel inverters.

However, the conventional virtual inductor method is generally implemented by making the output voltage reference proportional to derivation of inverter output current [16,17]. This method amplifies internal noises of output current. Therefore, a low-pass filter should be added into the virtual impedance loop so as to avoid introducing excessive noise to the control system. This method (LPF + LS method in short) works well for linear loads and nonlinear loads with smooth output current waveform. However, in the case of nonlinear load with severe distortion current waveform, the introduction of virtual impedance would bring harmonic amplification problems. Subsequently, it would deteriorate the performance of the virtual impedance loop. Eventually, the control system would be far beyond stability. Additionally, this method has a large calculation burden and slow dynamic response.

The method proposed in [18] can be used to solve some of the aforementioned problems. Its virtual impedance loop is implemented by a second-order generalized integrator, avoiding derivation of output current and reducing calculating burden. However, this method is not suitable for cases in which output current contains DC offset and severe distortion.

Nevertheless, the problems of DC offset and DC circulating current should not be ignored, as they would be damaging to the power supply system and electric equipment [19,20]. The following situations will add the DC component and DC circulating current to the inverter parallel system: 1) the power switches of each inverter cannot stay strictly synchronous, which will cause DC circulating current among inverters; 2) diode-rectified load will add the DC component problem in inverter output voltage; 3) the sampling process and analog-digital conversion of output voltage will also add the DC component; 4) the dead-time effect on the process of sinusoid pulse-width-modulation (SPWM) will also add the DC component.

In this paper, a current feedback control strategy for parallel inverters using a third-order general-integrator crossover-cancellation network that can be implemented in a virtual impedance loop is proposed to solve the aforementioned problem. This method consists of 2 parts: a crossover-cancellation feedback network and a multilevel orthogonal signal generator based on a third-order generalized integrator (TOGI). The first part realizes the decoupling effect among fundamental, DC, and harmonic components of the input signal. The second part extracts the fundamental orthogonal component of the input signal. Resistive, inductive, and complex virtual impedance can be achieved. The proposed method avoids differential of output current, reduces calculation burden, and increases dynamic response. The method can not only reduce the THD of output voltage in the case of nonlinear load, but can also drastically limit the impact of the DC component on output voltage. The simulation and experimental results verify the correctness and effectiveness of the proposed method.

2. Traditional droop control principle and concept of virtual impedance

Figure 1 shows the equivalent circuit schematic diagram of 2 inverters in parallel. $E_1\angle\varphi_1$ and $E_2\angle\varphi_2$ are the no-load output voltages of inverter 1 and inverter 2, respectively, and $U\angle 0$ is voltage at the point of common coupling (PCC).

Phase angle difference φ_i between the inverter output voltage and voltage of the PCC is generally very small, i.e. $\varphi_i \approx 0$, so $\sin\ \varphi_i \approx \varphi_i$, $\cos\ \varphi_i \approx 1$. Additionally, the distributed power generation system usually has inductive impedance, i.e. X_i is far larger than R_i; therefore, active power and reactive power output by the inverter are:

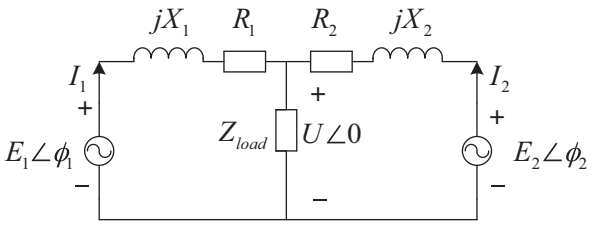

Figure 1. Equivalent circuit schematic diagram of 2 parallel inverters.

$$P_i \cong \frac{UE_i}{X_i}\phi_i, \tag{1}$$

$$Q_i \approx \frac{U}{X_i}(E_i - U). \tag{2}$$

Thus, traditional droop control characteristic can be expressed as:

$$\begin{cases} \omega_i = \omega_i^* - m * P_i \\ E_i = E_i^* - n * Q_i \end{cases}, \tag{3}$$

where m and n are droop coefficients for the frequency and amplitude, respectively.

To enhance system steady-state performance, reduce the influence of circulating current, and share linear and nonlinear loads, many methods introduce virtual impedance to the system through an additional control loop in the following form:

$$v_{ref} = v_{droop} - z_v(s)i_o, \tag{4}$$

where v_{droop} is the reference voltage obtained by the droop method, v_{ref} is the reference voltage after introduction of virtual impedance, and $z_v(s)$ is the virtual impedance.

3. Implementation of virtual impedance using the third-order general-integrator crossover-cancellation current feedback control method

3.1. Orthogonal signal generator based on TOGI

The structure diagram of an orthogonal signal generator (OSG) based on TOGI is shown in Figure 2. This structure requires a signal $v(t)$ and a frequency value ω_s as input and has 3 output signals; the closed-loop transfer functions are as follows:

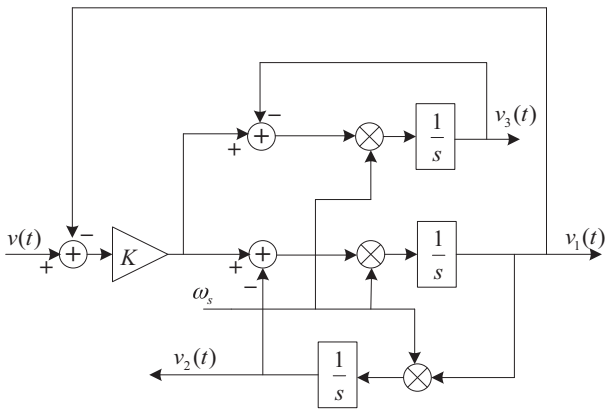

Figure 2. Block diagram of third-order generalized integrator.

$$F_1(s) = \frac{V_1(s)}{V(s)} = \frac{K\omega_s s}{s^2 + K\omega_s s + \omega_s^2}, \tag{5}$$

$$F_2(s) = \frac{V_2(s)}{V(s)} = \frac{K_s\omega_s^2}{s^2 + K\omega_s s + \omega_s^2}, \tag{6}$$

$$F_3(s) = \frac{V_3(s)}{V(s)} = \frac{K\omega_s(s^2 + \omega_s^2)}{(s+\omega_s)(s^2 + K\omega_s s + \omega_s^2)}, \tag{7}$$

where $V(s)$, $V_1(s)$, $V_2(s)$, and $V_3(s)$ represent the Laplace transformation of $v(t)$, $v_1(t)$, $v_2(t)$, and $v_3(t)$, respectively. As can be seen from Eqs. (5)–(7), the behavior of $F_1(s), F_2(s)$, and $F_3(s)$ in the frequency domain respectively act as a second-order band-pass filter, a second-order low-pass filter, and a band-stop filter.

Assume that input signal is a sinusoidal signal with a DC component and can be expressed as follows:

$$v(t) = A_0 + A_c \sin(\omega_c t + \phi_c). \tag{8}$$

Set resonant frequency of TOGI tuning at input signal frequency ω_c, i.e. $v_{3\infty}(t) = K_s A_0$, according to [21]; output signals of TOGI are:

$$v_{1\infty}(t) = A_c \sin(\omega_c t + \phi_c), \tag{9}$$

$$v_{2\infty}(t) = K_s A_0 - A_c \cos(\omega_c t + \phi_c), \tag{10}$$

$$v_{3\infty}(t) = K_s A_0. \tag{11}$$

According to Eqs. (8)–(11), $v_1(t)$ has the same amplitude and phase as the AC component of $v(t)$; term $v_1(t)$ is orthogonal to term $v_2(t) - v_3(t)$ and both terms contain no DC component in input signal; and $v_2(t) - v_3(t)$ has the same amplitude as $v_1(t)$, while its phase is 90° lagged behind. Figure 3 shows the structure of a 2-phase orthogonal signal generator constructed by TOGI (TOGI-OSG). Thus, TOGI-OSG could filter the DC component in the input signal and generate 2 orthogonal signals that have the same frequency and amplitude as the input fundamental component.

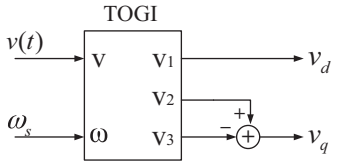

Figure 3. Block diagram of 2-phase orthogonal generator based on TOGI.

Additionally, according to Eqs. (5)–(7), TOGI-OSG includes a filtering harmonic function, but the filtering effects on low-order (such as 3rd, 5th, 7th, etc.) harmonics are not ideal and are easily affected by k value (see Section 4 for analysis of filtering performance of TOGI-OSG under the influence of the k value).

3.2. Crossover-cancellation feedback network based on TOGI-OSG

The crossover-cancellation feedback network based on TOGI-OSG, as depicted in Figure 4, consists of 2 parts: a crossover-cancellation feedback network, which achieves a band-pass effect, and a multilevel TOGI-OSG link, which acts as a filter. i_o is input current and i_1, i_3, i_5, and i_n are fundamental, 3rd, 5th, and nth harmonic current, respectively. Resonant frequency of the TOGI-OSG(n) is n times fundamental frequency. Even in the case of i_o containing the DC component and high THD, the proposed algorithm has the capacity to guarantee the extraction of the fundamental orthogonal component of i_o with less distortion. With the example of filtering the 3rd, 5th, and 7th harmonics (namely, n = 7), the transfer relationship between i_1 and i_o for TOGI-OSG (1), as depicted in Figure 4, is expressed as:

$$G(s) = \frac{k\omega s^7 + 83k\omega^3 s^5 + 1891k\omega^5 s^3 + 11025k\omega^7 s}{s^8 + 4k\omega s^7 + 84\omega^2 s^6 + 152k\omega^3 s^5 + (1974\omega^4 - 100k^2\omega^4)s^4 + 3848k\omega^5 s^3 + 12916\omega^6 s^2 + 12916k\omega^7 s + 11025\omega^8}. \tag{12}$$

The Bode diagram of Eq. (12) is shown in Figure 5. It is obvious that the amplitude response of Eq. (12) in the frequency domain around the 3rd, 5th, and 7th harmonics is largely decreased. This means that the 3rd, 5th, and 7th harmonics of i_0 are greatly attenuated.

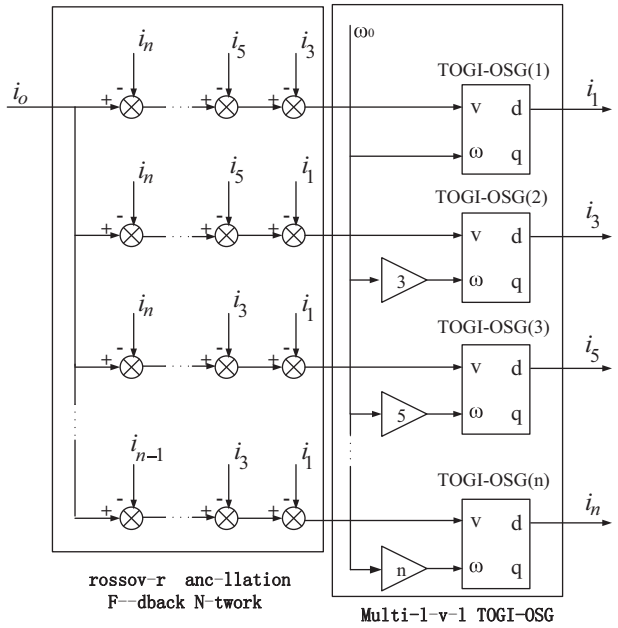

Figure 4. Block diagram of crossover-cancellation feedback network.

3.3. Implementation of virtual impedance using the proposed method in this paper

As analyzed above, the d output signal v_d of TOGI-OSG (1) in Figure 4 has the same amplitude and frequency as the fundamental component of the input signal, and the q output signal v_q is 90° lagged behind v_d where they both have the same amplitude. Assume that the expressions of both outputs are:

$$v_d(t) = A\sin(\omega t), \tag{13}$$

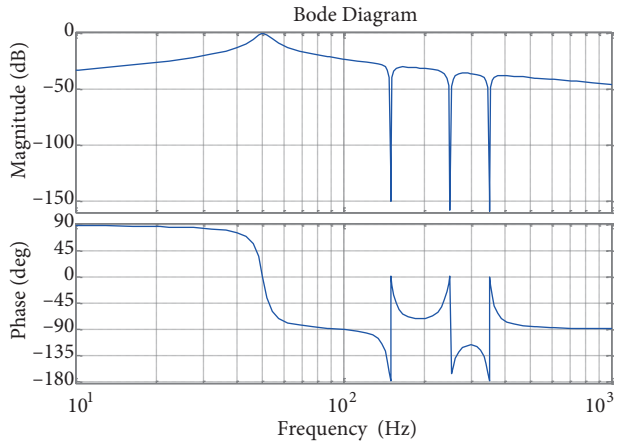

Figure 5. Bode diagram of closed-loop transfer function G(s).

$$v_q(t) = -A\cos(\omega t), \tag{14}$$

where A and ω are the amplitude and frequency of input signal, respectively. In view of expression of v_d, its virtual inductance value is:

$$z_v(t) = L_v \frac{dv_d(t)}{dt} = \omega L_v A\cos(\omega t). \tag{15}$$

With Eqs. (14) and (15), its virtual inductance value can be achieved by multiplying v_q by $-\omega$ and inductance value L, namely:

$$z_v(t) = -\omega L_v v_q(t). \tag{16}$$

Similarly, if the required virtual impedance is resistance, it can also be achieved easily by multiplying v_d by a resistance value, and the expression is as follows:

$$z_v(t) = R_v v_d(t). \tag{17}$$

Figure 6 shows the implementation diagram of inductive, resistive, and complex virtual impedance using the proposed method. In this figure, input signal ω comes from system frequency obtained by the droop control method.

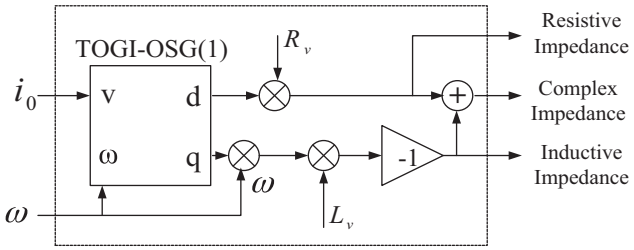

Figure 6. Implementation diagram of virtual impedance using the proposed method.

Thus, the proposed method in this paper avoids derivation of output current, reduces system calculation, enhances dynamic response, and greatly reduces the influence of noises, distortion, and DC offset in output current in the system.

4. Impact analysis of the proposed method in this paper on the system

Figure 7 shows the control diagram of a parallel inverters system. A double closed-loop feedback control strategy of an outer voltage loop and inner current loop is adopted: the outer loop uses a PI regulator to control output voltage tracking system reference voltage, so as to improve the waveform of system output voltage and obtain high output accuracy; the inner loop uses proportional control to improve the dynamic performance of the system.

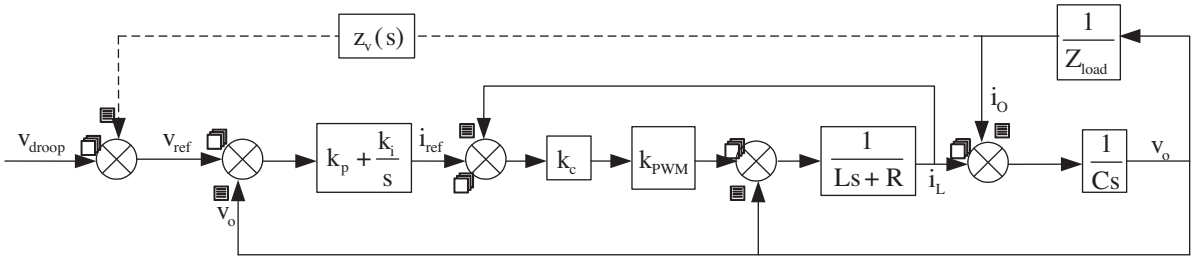

Figure 7. Diagram of parallel inverters control system.

Before introducing the virtual impedance $z_v(s)$ into the system, $v_{ref}(s) = v_{droop}(s)$, then: $v_o(s) = g(s)v_{ref}(s) - z_o(s)i_o(s)$, where

$$g(s) = \frac{k_c(k_p s + k_i)}{LCs^3 + C(r + k_c)s^2 + k_p k_c s + k_i k_c}, \tag{18}$$

$$z_o(s) = \frac{Ls^2 + rs}{LCs^3 + C(r + k_c)s^2 + k_p k_c s + k_i k_c}. \tag{19}$$

After introducing the virtual impedance $z_v(s)$, the voltage reference of the system can be expressed as $v_{ref}(s) = v_{droop}(s) - z_v(s)i_o(s)$; thus, inverter equivalent output impedance can be expressed as $z_o^*(s) = z_o(s) + g(s)z_v(s)$.

Figures 8a–8c show the Bode diagrams of total system output impedance using the traditional LPF+LS method, the SOGI method proposed in the literature [18], and the third-order general-integrator crossover-cancellation current feedback control method proposed in this paper, respectively. These Bode diagrams are obtained with the following parameters: $k_p = 0.8, k_i = 350, k_c = 3.5, \omega = 100\pi rad/s, L = 1.36mH$,

$$R = 0.8\Omega, C = 11\mu F, k = 1.$$

In Figure 8, solid lines denote Bode diagrams of the original output impedance of the inverter without virtual impedance, while dotted lines denote Bode diagrams of total equivalent output impedance after adding virtual impedance using different methods. According to Figure 8a, after adding virtual impedance using the LPF+LS method to the system, almost the entire frequency band in the Bode diagram is affected; that is to say, virtual inductance value has an effect on system harmonic gain, and its increase would result in the increase of harmonic gain. As can be seen from Figure 8b, after adding virtual impedance using the SOGI method to the system, only output impedance around the fundamental frequency is affected, and output impedance at harmonic frequency will not be affected; however, this method cannot suppress the DC offset of the system. In Figure 8c, Z_o is the Bode diagram of the original output impedance of the inverter without virtual impedance; Z_{ov} ($L_v = 4$ mH) and Z_{ov} ($L_v = 5$ mH) are Bode diagrams of total system output impedance after adding virtual inductance, the values of which are 4 mH and 5 mH, respectively, implemented by the method proposed in this paper. As

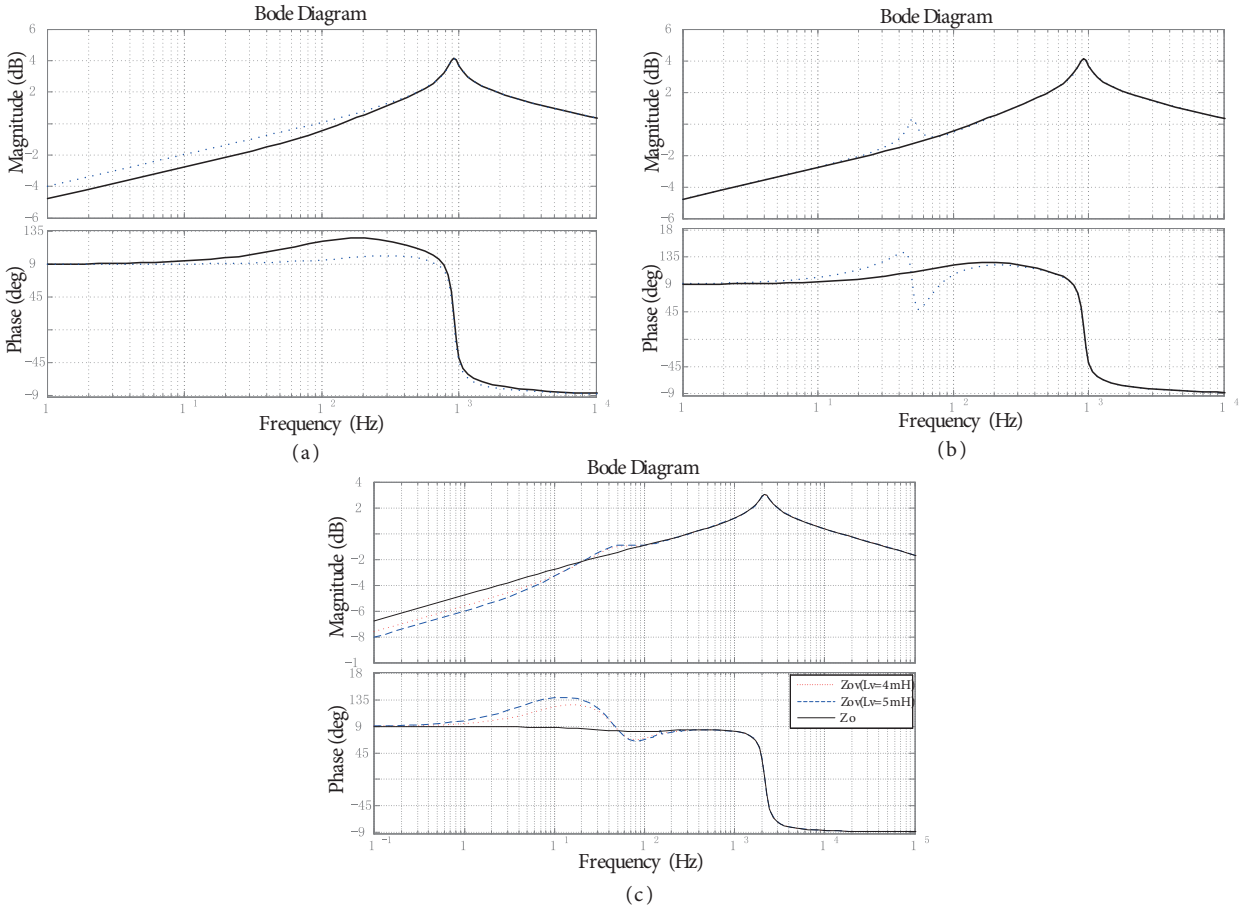

Figure 8. Bode diagram of inverter total output impedance: (a) with LPF+LS method; (b) with SOGI method; (c) with the proposed method.

can be seen in the figure, the total output impedance has certain attenuation at DC, and only output impedance around the system's fundamental frequency is affected, while output impedance at the harmonics frequency will not be affected. Thus, the proposed virtual impedance implementation method performs well in suppressing the effect of the DC component and harmonic component in output current on the system.

5. Simulation and experimental results

5.1. Analysis of the influence of k value on TOGI-OSG filtering performance

Figure 9a shows the time response of TOGI-OSG to sinusoidal input current signal with high-frequency noise, a current amplitude of 6 A, and a DC offset of 1 A when k is 1 and 0.1, respectively. It can be seen that 2 orthogonal output signals of TOGI-OSG will not be affected by input noise or DC offset. Figure 9b shows the time response of TOGI-OSG to input current signal with harmonic component, a current amplitude of 8 A, and a DC offset of 1 A when k is 1 and 0.1, respectively. As can be seen in this figure, TOGI-OSG can suppress harmonics to a certain degree; the value of k determines dynamic response speed and harmonic suppression ability of TOGI-OSG. Greater k means quicker dynamic response speed and weaker harmonic suppression ability, while, on the contrary, smaller k means slower dynamic response speed and stronger harmonic suppression ability. Thus, the value of k shall be reasonably set in order to make the system have good filtering function and dynamic performance while ensuring system stability.

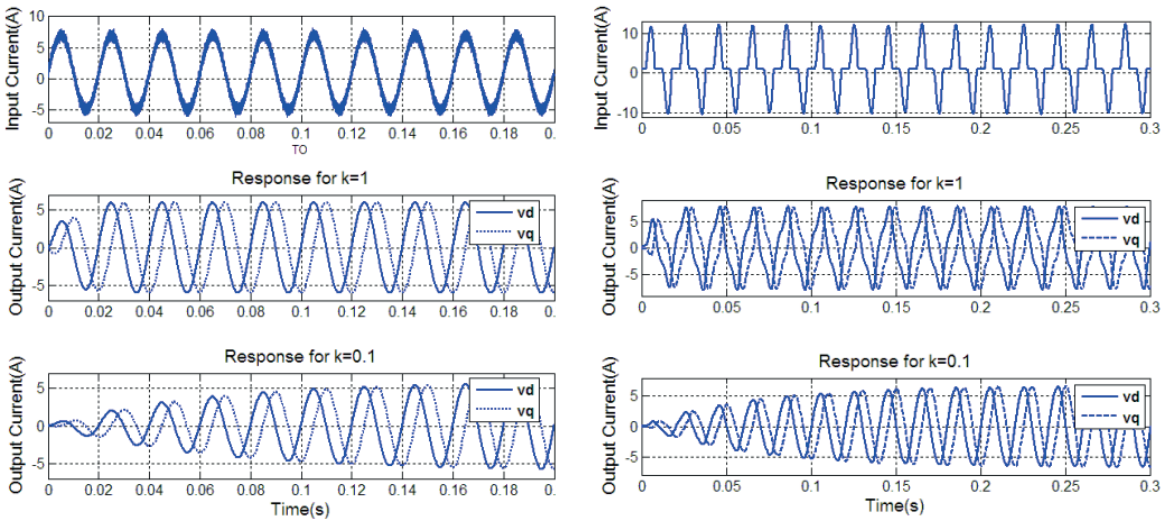

Figure 9. TOGI-OSG time response for different input signals: (a) for the sinusoidal input with high-frequency noise and DC offset when k = 1 and k = 0.1; (b) for the nonlinear input with harmonic and DC offset when k = 1 and k = 0.1.

5.2. Analysis of filtering characteristics of the proposed method in this paper

Figure 10 shows time response using the method proposed in this paper to input current signal with harmonic component, an amplitude of 8 A, and a DC offset of 1 A when k = 1. Table 1 lists harmonic contents and the total harmonic distortion (THD) (3 decimal places) after filtering of the input signal shown in Figure 10 by the TOGI-OSG method when k is 0.1 and 1, respectively, and the proposed method in this paper when k = 1. As can be seen from Figure 10 and Table 1, the proposed method in this paper solves the problem of a compromised setting of the k value with consideration of the filtering performance and dynamic performance of the TOGI-OSG method, and it has ideal effects in filtering harmonics and DC component even with a larger value of k; thus, it achieves good dynamic response and harmonic suppression ability.

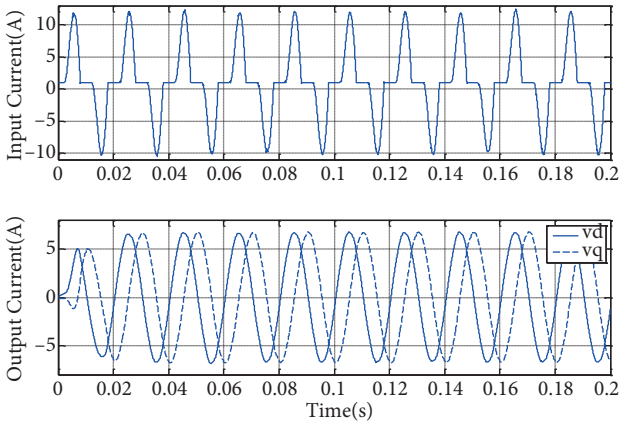

Figure 10. Time response of crossover-cancellation feedback network based on TOGI-OSG for input signals with harmonic and DC component when k = 1.

Table 1. Comparison of 2 methods of filtering effect.

		Fundamental	3rd	5th	DC	THD
Input signal		6.721	3.852	0.904	1.019	59.46%
TOGI method (k = 1)	V_d	6.732	1.353	0.182	0.006	20.31%
	V_q	6.734	1.353	0.182	0.004	20.30%
TOGI method (k = 0.1)	V_d	6.621	0.152	0.024	0.004	2.23%
	V_q	6.611	0.151	0.024	0.004	2.23%
The proposed method (k = 1)	V_d	6.721	0.011	0.002	0.002	0.56%
	V_q	6.721	0.011	0.002	0.002	0.56%

5.3. Experimental results

As shown in Figure 11, the experiment was conducted on a system platform with 2 parallel inverters built in the laboratory; the rated power of both inverters is 2 kW. Each inverter consists of a single-phase IGBT full-bridge circuit with switching frequency of 12.8 kHZ and an LC output filter. The system parameters are shown in Table 2.

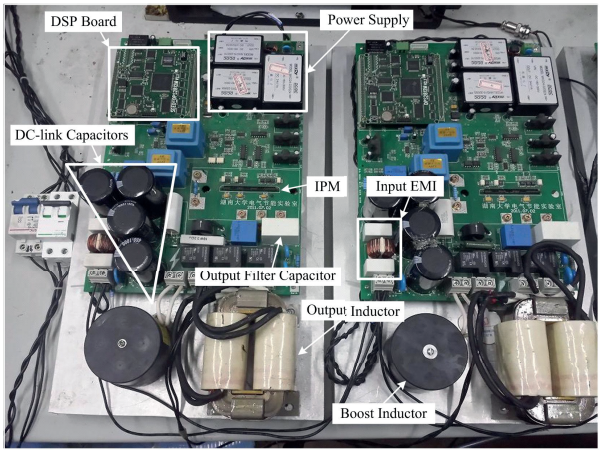

Figure 11. Experimental platform with 2 parallel inverters.

Table 2. Experimental parameters.

Parameter	Value	Parameter	Value
E^*/V	220	L/mH	1.36
f_0/Hz	50	R/Ω	0.8
f_c/kHz	12.8	C/mu F	11
k_p	0.8	k	1
k_i	350	L_v/mH	4
k_c	3.5	ω_c/rad/s	150 × 2π

Figure 12 shows experimental waveforms of the 2 parallel inverters when sharing linear RL load (R = 15 Ω, L = 80 mH) using the proposed method in this paper; the DC signal, which is 2% of the peak value of the modulation signal, is artificially overlapped on the PWM modulation signal to further verify that this method could suppress the influence of DC circulating current and DC offset on system output voltage. As can be seen in Figure 12a, the circulating current between the 2 inverters is quite small, and the amplitude of the

circulating current is less than 0.1 A. As can be seen in Figure 12b, there is no DC offset in the output voltage. Therefore, the method proposed could work well for sharing linear load and restraining the influence of the DC component on output voltage.

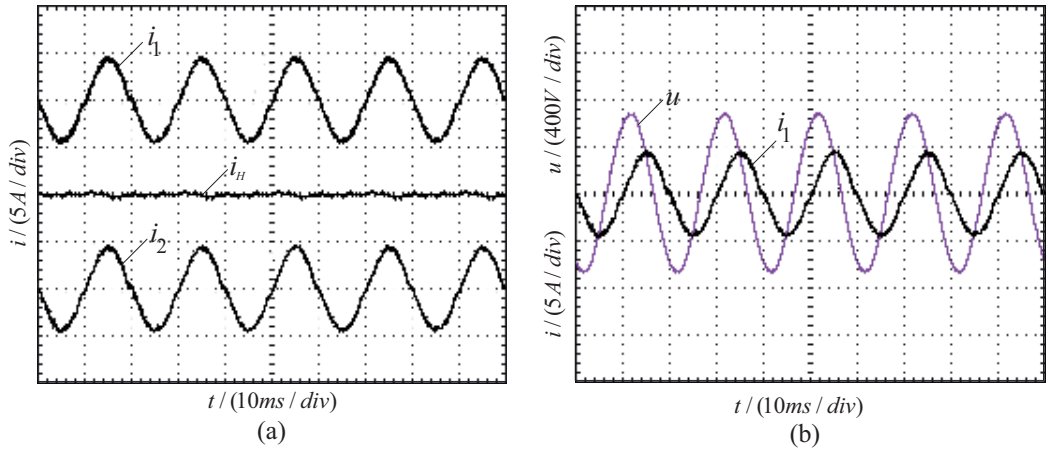

Figure 12. Experimental waveforms with linear load: (a) output current and circulating current of parallel inverters; (b) output voltage and current of inverter 1.

Figure 13 shows experimental waveforms of 2 parallel inverters when sharing nonlinear load using the proposed method in this paper; nonlinear uncontrollable rectifier load with rated power of 1.6 kVA is used as the nonlinear load. As can be seen in the figure, 2 inverters could share nonlinear load very well, and circulating current between the 2 inverters is very small.

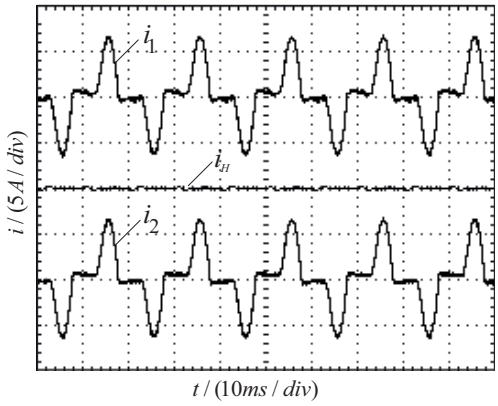

Figure 13. Experimental waveforms of 2 inverters in parallel with nonlinear loads.

Figures 14a–14c show experimental waveforms of output voltage and current using the LPF+LS method, the SOGI method, and the method proposed in this paper, respectively, when the system shares an uncontrollable rectifier nonlinear load. The spectrum analysis of output voltage in Figures 14a–14c was conducted by Fluke analyzer; the FFT diagrams are shown in Figures 15a–15c. As can be seen from Figure 15, the THD of output voltage using the LPF+LS method, the SOGI method, and the method proposed in this paper is 9.4%, 3.7%, and 2.3%, respectively. The THD of output voltage by the proposed method in this paper is the lowest, which is consistent with the simulation results.

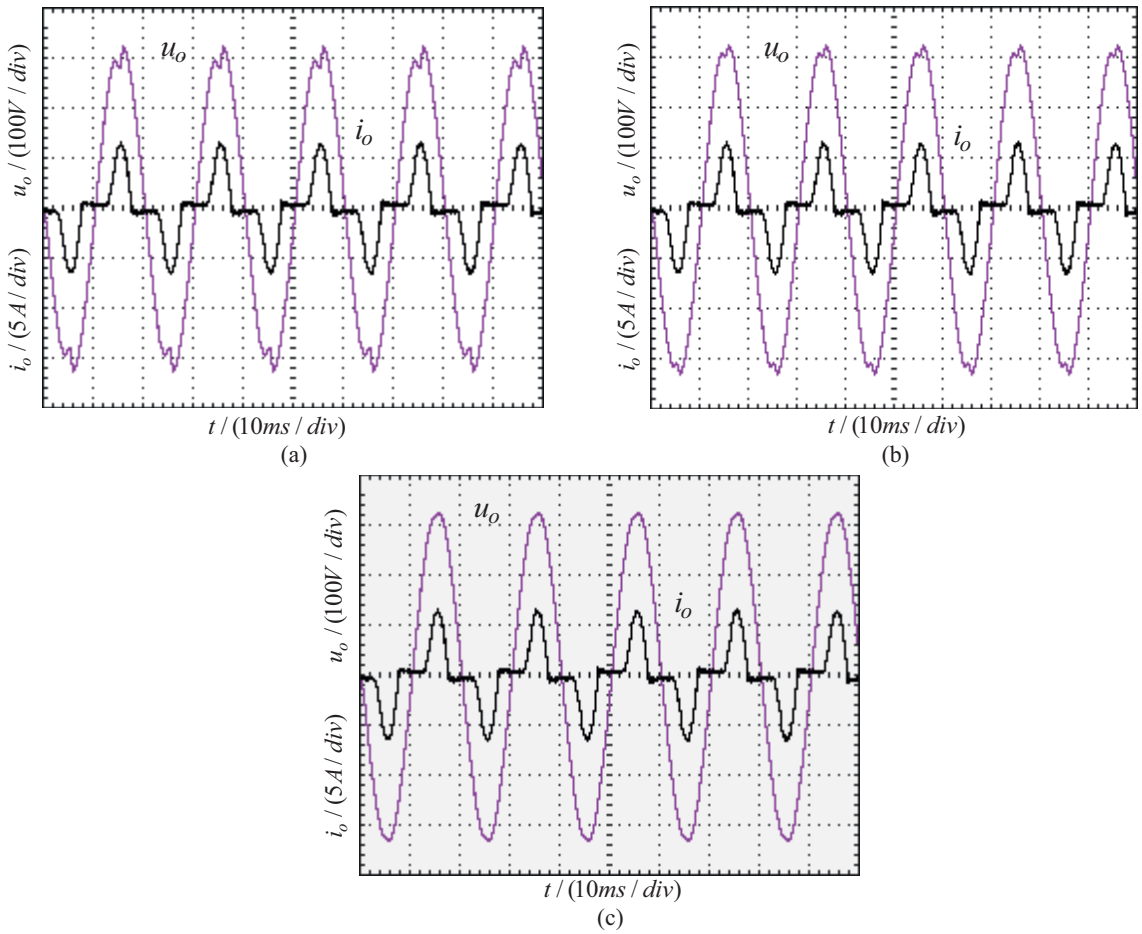

Figure 14. Experimental waveforms of 1 inverter with nonlinear load: (a) using LPF+LS method; (b) using SOGI method; (c) using the method proposed in this paper.

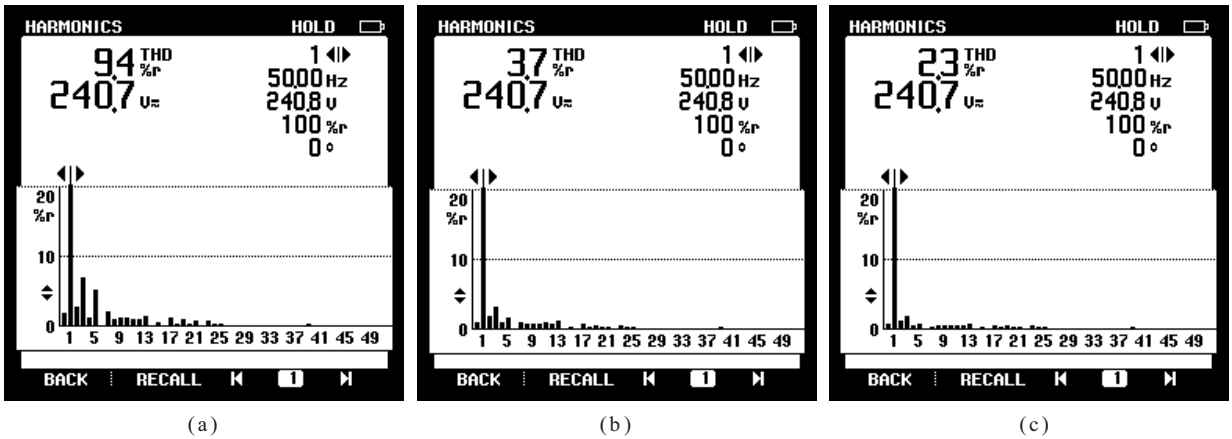

Figure 15. Spectrogram of output voltage: (a) using LPF+LS method; (b) using SOGI method; (c) using the method proposed in this paper.

6. Conclusion

In this paper, a current feedback control strategy for parallel inverters using a third-order general-integrator crossover-cancellation network implemented in virtual impedance is proposed, which avoids derivation of output current, reduces system calculation, and enhances system response. The proposed method consists of 2 parts: a crossover-cancellation feedback network, which achieves band-pass effects, and a multilevel TOGI–OSG link, which achieves filtering function. This method has excellent effects on suppressing the DC component in output current and could improve output voltage waveforms and reduce the THD of output voltage. In addition, this method also has advantages including easy implementation, quick and accurate signal tracking ability, and effective suppression of noises in the input signal. Simulated and experimental results have demonstrated the good performance of the method.

References

[1] Yazdanian M, Sani AM. Distributed control techniques in microgrids. IEEE T Smart Grid 2014; 5: 2901-2909.

[2] Rocabert J, Luna A, Blaabjerg F, Rodriguez P. Control of power converters in AC microgrids. IEEE T Power Electron 2012; 27: 4734-4749.

[3] Olivares DE, Sani AM, Etemadi AH, Canizares CA, Iravani R, Kazerani M, Hajimiragha AH, Bellmunt OG, Saeedifard M, Behnke RP et al. Trends in microgrid control. IEEE T Smart Grid 2014; 5: 1905-1919.

[4] Guerrero JM, Vicuña LG, Matas J, Castilla M, Miret J. A wireless controller to enhance dynamic performance of parallel inverters in distributed generation systems. IEEE T Power Electron 2004; 19: 1205-1213.

[5] Vasquez JC, Guerrero JM, Savaghebi M, Garcia JE, Teodorescu R. Modeling, analysis, and design of stationary-reference-frame droop-controlled parallel three-phase voltage source inverters. IEEE T Ind Electron 2013; 60: 1271-1280.

[6] Hasanzadeh A, Onar OC, Mokhtari H, Khaligh A. A proportional-resonant controller-based wireless control strategy with a reduced number of sensors for parallel-operated UPSs. IEEE T Power Deliver 2010; 25: 468-478.

[7] Zhong QC. Robust droop controller for accurate proportional load sharing among inverters operated in parallel. IEEE T Ind Electron 2013; 60: 1281-1290.

[8] Tao Y, Liu QW, Deng Y, Liu XH, He XN. Analysis and mitigation of inverter output impedance impacts for distributed energy resource interface. IEEE T Power Electron 2015; 30: 3563-3576.

[9] Guerrero JM, Vasquez JC, Matas J, Castilla M, Vicuna LG. Control strategy for flexible microgrid based on parallel line-interactive UPS systems. IEEE T Ind Electron 2009; 56: 726-736.

[10] He JW, Li YW. Generalized closed-loop control schemes with embedded virtual impedances for voltage source converters with LC or LCL filters. IEEE T Power Electron 2012; 27: 1850-1861.

[11] Guerrero JM, Matas J, Vicuña LG, Castilla M, Miret J. Decentralized control for parallel operation of distributed generation inverters using resistive output impedance. IEEE T Ind Electron 2007; 54: 994-1004.

[12] Li YW, Kao CN. An accurate power control strategy for power-electronics-interfaced distributed generation units operating in a low-voltage multibus microgrid. IEEE T Power Electron 2009; 24: 2977-2988.

[13] He JW, Li YW. Analysis, design, and implementation of virtual impedance for power electronics interfaced distributed generation. IEEE T Ind Appl 2011; 47: 2525-2538.

[14] Zhang Y, Yu M, Liu FR, Kang Y. Instantaneous current-sharing control strategy for parallel operation of UPS modules using virtual impedance. IEEE T Power Electron 2013; 28: 432-440.

[15] Kim J, Guerrero JM, Rodriguez P, Teodorescu R, Nam K. Mode adaptive droop control with virtual output impedances for an inverter-based flexible AC microgrid. IEEE T Power Electron 2011; 26: 689-701.

[16] Guerrero JM, Vicuña LG, Matas J, Castilla M, Miret J. Output impedance design for parallel-connected UPS inverters with wireless load sharing control. IEEE T Ind Electron 2005; 52: 1126-1135.

[17] Yao W, Chen M, Matas J, Guerrero JM, Qian ZM. Design and analysis of the droop control method for parallel inverters considering the impact of the complex impedance on the power sharing. IEEE T Ind Electron 2011; 58: 576-586.

[18] Matas J, Castilla M, Vicuña LG, Miret J, Vasquez JC. Virtual impedance loop for droop-controlled single-phase parallel inverters using a second-order general-integrator scheme. IEEE T Power Electron 2010; 25: 2993-3002.

[19] Bowtell L, Ahfock A. Direct current offset controller for transformerless single-phase photovoltaic grid-connected inverters. IET Renew Power Gen 2010; 4: 428-437.

[20] He GF, Xu DH, Chen M. A novel control strategy of suppressing DC current injection to the grid for single-phase PV inverter. IEEE T Power Electron 2015; 30: 1266-1274.

[21] Fedele G, Ferrise A, Muraca P. An adaptive quasi-notch filter for a biased sinusoidal signal estimation. In: 2011 9th IEEE International Conference on Control and Automation; 19–21 December 2011; Santiago, Chile. Piscataway, NJ, USA: IEEE. pp. 1060-1065.